

1 **Contributions of primary emissions and secondary formation to nitrated aromatic**
2 **compounds in mountain background region of Southeast China**

3
4 Yanqin Ren¹, Gehui Wang², Jie Wei³, Jun Tao⁴, Zhisheng Zhang⁴, Hong Li¹
5
6
7
8
9

10 ¹State Key Laboratory of Environmental Criteria and Risk Assessment, Chinese
11 Research Academy of Environmental Sciences, Beijing 100012, China

12 ²Key Lab of Geographic Information Science of Ministry of Education of China,
13 School of Geographic Sciences, East China Normal University, Shanghai 200142,
14 China

15 ³Key Laboratory of Ecosystem Network Observation and Modeling, Institute of
16 Geographic Sciences and Natural Resources Research, Chinese Academy of
17 Sciences, Beijing 100101, China

18 ⁴South China Institute of Environmental Sciences, Ministry of Ecology and
19 Environment, Guangzhou, 510655, China
20
21

22 Correspondence: Gehui Wang (ghwang@geo.ecnu.edu.cn) and Jie Wei
23 (weijie@igsnr.ac.cn)
24
25
26
27
28

29 **Abstract**

30 As a major component of brown carbon (BrC), nitrated aromatic compounds (NACs)
31 have a significant role in the atmosphere's ability to absorb light. However, the sources
32 and major influencing factors of NACs in the mountain background atmosphere are
33 mostly lacking. Based on a thorough field investigation of NACs from fine particle
34 samples taken in 2014 and 2015 at the peak of Mt. Wuyi (1139 meters above sea level),
35 the current work discussed the seasonal fluctuations in their composition, sources, and
36 the important influencing factors. The total abundance of nine quantifiable NACs
37 increased significantly in the winter ($3.9 \pm 1.5 \text{ ng m}^{-3}$) and autumn ($2.1 \pm 0.94 \text{ ng m}^{-3}$),
38 whereas it decreased in the spring ($1.3 \pm 0.75 \text{ ng m}^{-3}$) and summer ($0.97 \pm 0.36 \text{ ng m}^{-3}$).
39 According to the results of structural equation modeling, the majority of NACs (93%)
40 were influenced by biomass, coal, and petroleum combustion over the entire year. This
41 work identified the origins of NACs with applying the Positive Matrix Factorization
42 receptor model. The five major source factors were biomass burning, coal combustion,
43 secondary formation by nitration reaction, secondary formation by photochemical
44 reaction, and other sources. Among them, biomass burning and coal combustion played
45 an important role, especially in the wintertime, with a contribution of more than 50%.
46 Meanwhile, contributions from secondary formation were significant in this remote
47 areas, which mainly by photochemical reaction in the summertime, and nitration
48 reaction in the wintertime. Further analysis indicated that the formation of NACs was
49 comparatively sensitive to NO_2 under low- NO_x conditions, suggesting that NACs

50 would become significant in the aerosol characteristics when nitrate concentrations
51 decreased as a result of emission reduction measures.

52 **1 Introduction**

53 Nitrated aromatic compounds (NACs) are kinds of the most important constituents
54 of BrC, which have an aromatic moiety and the -OH and -NO₂ functions (Desyaterik et
55 al., 2013; Wu et al., 2020). Nitrophenols (NPs), nitrosalicylic acids (NSAs),
56 nitroguaiacols (NGAs), and nitrocatechols (NCs) are the most common among various
57 kinds of NACs. Due to their capacity to absorb light, they have received a lot of
58 attention (Li et al., 2020c; Wang et al., 2018; Teich et al., 2017; Wang et al., 2016).
59 About 4% of the net water-soluble BrC absorption has been ascribed to them as
60 documented by several earlier studies (Mohr et al., 2013; Zhang et al., 2013). Moreover,
61 they manifest an influence on human health, because of NACs' strong mutagenicity,
62 cytotoxicity, and carcinogenicity (Iinuma et al., 2010).

63 Various ambient atmospheres has been shown to have NACs, including rural
64 (Liang et al., 2020; Teich et al., 2017; Lv et al., 2022), urban (Li et al., 2020b; Li et al.,
65 2020c; Wang et al., 2019; Ren et al., 2022; Li et al., 2020a), suburban (Kitanovski et
66 al., 2021), and mountain (Wang et al., 2018). Biomass burning (Wang et al., 2017; Lin
67 et al., 2017; Chow et al., 2015; Gaston et al., 2016; Salvador et al., 2021), traffic
68 emissions (Lu et al., 2019a), and coal combustions (Lu et al., 2019b) are the key
69 primary sources of NACs. Several works indicated that the primary cause of the
70 generation of NACs is biomass burning (Lin et al., 2017; Wang et al., 2017; Mohr et

71 al., 2013), whereas several other studies consider road traffic emissions as the primary
72 cause of the origin of nitrophenols (Zhang et al., 2010). Secondary formation is also a
73 very important source of particulate NACs although NACs are highly affected by
74 primary emissions, and NO₂ is a very important factor during the process (Ren et al.,
75 2022; Cai et al., 2022; Cheng et al., 2021). Secondary chemistry primarily classified as
76 the nitration of aromatic compounds, may occur in both aqueous and gas phases (Li et
77 al., 2020c; Harrison et al., 2005; Wang et al., 2019). According to recent research,
78 phenolic VOCs being oxidized by the nitrate radical (NO₃•) at night may also function
79 as a notable source of nitrophenols and additional BrC species (Mayorga et al., 2021).
80 Studies have revealed that there is a closer link between NACs and NO₂ for samples
81 taken at night, further pointing to the importance of NO₃•-initiated oxidation in the
82 generation of NACs at night (Wang et al., 2018; Li et al., 2020c; Cai et al., 2022).
83 According to the previous research, the intermediate formed when phenol reacts with
84 either •OH during in the daytime or NO₃• during the night produces phenoxy radical
85 (C₆H₅O•), which is where nitrophenol is produced (Berndt and Bge, 2003). Even
86 though researchers have started to study NACs, very little is known regarding the
87 relative significance of their corresponding primary and secondary sources. The
88 fundamental variables affecting the generation of NACs are also little known because
89 only a few investigations have been conducted thus far, in particular within China.

90 Field observations in both clean and polluted environments are essential for better
91 identifying elements that have previously gone unnoticed and for confirming the
92 mechanistic understanding attained from research on smog chambers. In our earlier

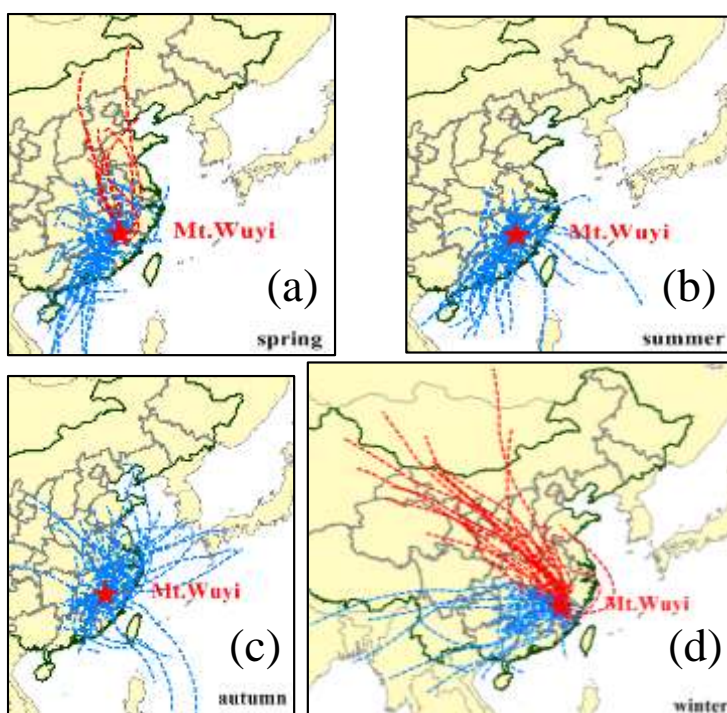
93 research, we examined how biomass burning affects biogenic secondary organic
94 aerosol (BSOA) production from long-range transport and how biogenic volatile
95 organic compounds (BVOCs) contribute to the generation of BSOA in high mountain
96 locations, which proved the effect of long-range transport of air pollutants (Ren et al.,
97 2019). In the current study, nine NACs (NPs, NGAs, NCs, and NSAs) in the PM_{2.5} were
98 studied at the same sampling site, to further understand ambient characteristics of NACs,
99 their primary sources, and the principal factors influencing their secondary formation
100 in the mountain background region. The outcome of the current research offers useful
101 insight into the pollution characteristics and sources of NACs, and the potential
102 influences on the second formation in background environments.

103 **2 Materials and methods**

104 **2.1 Sample site and field observations**

105 One national atmospheric background monitoring station is located at Mt. Wuyi
106 station (27°35'N, 117°43'E, 1139 m a.s.l., Fig. 1). There are no evident sources of
107 atmospheric pollution within 50 km² of the monitoring station, which is located at the
108 southern tip of the Mt. Wuyi national reserve. As a result, it can accurately depict the
109 atmospheric background conditions of southeast China's forest and mountain region.
110 Due to its high altitude and active airstream, it can also be used to observe the effects
111 of long-range transport. In this work, we used a high-volume air sampler (TE-6070DV-
112 BLX, Tisch Environmental Inc., USA) to gather PM_{2.5} samples with an airflow
113 equivalent to 1.13 m³ min⁻¹. 49 PM_{2.5} samples in total were taken over seven days.

114 During the sampling, four blank specimens (one for individual seasons) were obtained
115 by mounting the filters onto the sampler without pumping any air. The samples and
116 blanks were collected onto pre-combusted quartz filter (450°C for 8 h). After the
117 sampling and before any analysis, all filters were sealed individually in an aluminum
118 bag, and stored in a freezer below -18°C. At the same time, we gathered data on
119 conventional pollutants and meteorological parameters, including temperature (T),
120 relative humidity (RH), SO₂, NO₂, and O₃. The meteorological data were monitored by
121 a Vaisala MAWS301 (Helsinki, Finland) automatic weather station, and the
122 conventional pollutants were monitored with a model 43i SO₂ analyzer for SO₂, a model
123 17i NH₃ analyzer for NO₂, and a model 49i O₃ analyzer for O₃ (Thermo Scientific
124 Company, Waltham, MA, USA). Sample site and sampling information has been
125 reported in detail in the literature (Ren et al., 2019).



126
127 Fig. 1 Location of the sampling site (Mt. Wuyi: 27°35' N, 117°43' E; 1139 m a.s.l.)
128 and 48-hour backward trajectories reaching the summit during the sampling (spring:
129 March 20, 2014- June 4, 2014; summer: June 4, 2014- September 2, 2014; autumn:

130 September 2, 2014-December 4, 2014; winter: December 4, 2014- February 25, 2015.
131 Red dotted line: the air masses coming from north and northwest; Blue dotted line: the
132 air masses coming from other directions).

133 2.2 Chemical analysis

134 Organic compounds, including nine NACs (3-methyl-4-nitrophenol (3M4NP), 4-
135 nitrophenol (4NP), 2,4-dinitrophenol (2, 4-DNP), 4-nitroguaiacol (4NGA), 5-
136 nitroguaiacol (5NGA), 4-nitrocatechol (4NC), 4-methyl-5-nitrocatechol (4M5NC), 3-
137 nitro-salicylic acid (3NSA), and 5-nitro-salicylic acid (5NSA)), fossil fuel *n*-alkanes (ff
138 *n*-alkanes), PAHs, and sugars (e.g. trehalose, and levoglucosan), were identified in the
139 samples. Elemental carbon (EC), organic carbon (OC) and some inorganic ions (i.e.
140 SO_4^{2-} , NO_3^- , NH_4^+ , K^+) were also the constituents of the samples. The procedures for
141 sample extraction and derivatization have been elaborated elsewhere (Ren et al., 2022;
142 Ren et al., 2019). Briefly stated, an aliquot of the filter was extracted with a mixture of
143 methanol and dichloromethane (DCM, 1:2) under ultrasonication for three times. The
144 extracts are concentrated and dried by using pure nitrogen, derivatized with N, O-bis-
145 (trimethylsilyl) trifluoroacetamide (BSTFA), and analyzed by using gas
146 chromatography equipped with mass spectroscopy (GC-MS, 7890A/5975C, Agilent
147 Co., USA). The GC separation was carried out on a DB-5MS fused silica capillary
148 column, and the GC oven temperature programmed from 50°C (2min) to 120°C with
149 15°C min⁻¹ and then to 300°C with 5°C min⁻¹, with a final isothermal hold at 300°C for
150 16 min. The sample was injected in a splitless mode at an injector temperature of 280°C,
151 and scanned from 50 to 650 Daltons using electron impact (EI) mode at 70eV. Using
152 the Interagency Monitoring of Protected Visual Environments (IMPROVE)

153 thermal/optical reflectance (TOR) methodology, OC and EC were measured by a DRI
154 model 2001 Carbon Analyze (Atmoslytic Inc., Calabasas, CA, USA). OC collected by
155 filter membrane are first volatilized with the proceeding of temperature up to 580 °C in
156 the protection of He and determined. EC are analyzed then with the increasing of
157 temperature to 840°C in the presence of He and O₂ by the NDIR non-dispersive infrared
158 CO₂ detector. Dionex-600 ion chromatography was used to quantify inorganic ions in
159 samples after extracted with Mili-Q pure water (Thermo Fisher Scientific Inc., USA).

160 **2.3 Model calculation**

161 As a receptor model, Positive Matrix Factorization (PMF) (EPA PMF 5.0 version)
162 has been extensively employed for the source distribution of atmospheric pollutants
163 (Ren et al., 2022; Wu et al., 2020; Wang et al., 2018). To quantify the source
164 apportionment for NACs, the mass concentrations of SO₂, NO₂, CO, O₃, sulfate (SO₄²⁻),
165 nitrate (NO₃⁻), NH₄⁺, K⁺, ff-*n*-alkanes, PAHs, levoglucosan, trehalose, 3M4NP, 4NP,
166 4NGA, 5NGA, 2,4-DNP, 4M5NC, 4NC, 5NSA, and 3NSA, were employed as input
167 data. The direct and indirect effects of air pollutants variables on NACs were quantified
168 by utilizing structural equation modeling (SEM). Initially, a conceptual model of
169 hypothetical linkages was developed using past and theoretical information. The
170 measured data were then integrated into the model using the maximum-likelihood
171 estimation technique. AMOS 24.0 (IBM, Chicago, IL, USA) was used to analyze the
172 above statistical analyses.

173 2.4 Quality assurance and quality control (QA/QC)

174 For pre-treatment experiments, all glassware used were rinsed and baked at 450 °C
175 for 8 h and further cleaned by using methanol, DCM and hexane immediately before
176 using. Limit of detection (L.O.D.) of the target compounds were calculated with signal-
177 to-noise ratios of 3:1, according to the method reported by previous studies (Bandowe
178 et al., 2014; Li et al., 2016). In this work L.O.D. of NAC species were in the range of
179 0.0001-0.002 (Table S1). Field blank sample analysis showed no serious contamination
180 (less than 5% of real samples). GC/MS response factors of all organic species were used
181 those of the authentic standards. The recovery experiment was done by spiking the
182 standard solution onto blank filters (n=3) and analyzed using the above procedure.
183 Recoveries of the quantified organic compounds were generally between 80% and
184 110%. Data reported here were all corrected for the blanks.

185 For PMF, the model was iterated upon using a variety of combinations of the
186 concentration data set and three to six covariates. Q value and r , which were defined as
187 the agreement between the model fit and the correlation between estimated and
188 measured concentrations, respectively, are used to determine the appropriate factor
189 number for modeling (Comero et al., 2009). The best solution was determined to be
190 five components based on the Q value and r^2 (Table S2) values. For SEM, we identified
191 the model that best fits the data by methodically deleting non-significant routes from
192 the base model. The p -value, χ^2 -test, goodness-of-fit index (GFI) and root mean square
193 error of approximation (RMSEI) index were used to assess the model's suitability. The
194 conceptual model was acceptable if the p -value > 0.05 , Low RMSEA (< 0.08), high GFI

195 (>0.9), and low χ^2 values were regarded as positive model fits. In this work, the model
196 fits the data well, i.e. $\chi^2 = 0.235$, $df=1$, $p=0.628$, $GFI=0.999$, and $RMSEA=0.000$ in
197 annual); $\chi^2 = 0.690$, $df=2$, $p = 0.708$, $GFI=0.980$, and $RMSEA=0.000$ in winter.

198 **3 Results and discussion**

199 **3.1 Meteorological Features and Air masses**

200 From March 2014 through February 2015, a total of four seasons were covered by
201 the sampling campaign. In the area under investigation, the four seasons are typically
202 referred to as spring (March through May), summer (June through August), autumn
203 (September through November), and winter (December through February). The rise in
204 temperature starts in March, and peaks in July (25 °C), before falling to a minimal value
205 of 2.9 °C in January–February. When determining the origin of air masses at a certain
206 location, air mass backward trajectories are taken into account. The Hybrid Single-
207 Particle Lagrangian Integrated Trajectories (HY-SPLIT) model supplied 48-hour air
208 mass backward trajectories for this study. The source regions of primary aerosol
209 gathered from an area located at a distance from the source location, have been also
210 identified using air mass backward trajectories (Chiapello et al., 1997; Wang et al., 2013;
211 Wang et al., 2014). The 48-hour backward trajectories (Fig. 1) show that during the
212 sampling, winds from the north were reaching the top, particularly in winter (Fig. 1d),
213 when there were large concentrations of air pollutants due to anthropogenic emissions.
214 This explains why SO₂, NO₂, ff-*n*-alkanes (fossil fuel markers), PAHs (coal and fossil
215 fuel markers), levoglucosan (biomass burning markers), SO₄²⁻, NO₃⁻, and other

216 anthropogenic pollutants were typically higher in winter (Table 1). This has been
217 demonstrated in our previous studies that these anthropogenic pollutants can affect the
218 generation of certain SOA species (Ren et al., 2019).

Table 1. Concentrations (ng m^{-3}) of organic compounds in $\text{PM}_{2.5}$ samples in Mt. Wuyi during the sampling time.

	spring (n=11)	summer (n=13)	autumn (n=13)	winter (n=12)
$\text{PM}_{2.5}$ ($\mu\text{g m}^{-3}$)	16 \pm 5.5 (7.6-24) ^b	14 \pm 7.8 (4.9-32)	20 \pm 7 (8.3-31)	21 \pm 7.8 (5-32)
T ($^{\circ}\text{C}$)	16 \pm 3.6 (8.2-21)	23 \pm 1.3 (21-25)	17 \pm 4.7 (9.6-23)	6.4 \pm 2.8 (2.9-11)
RH (%)	78 \pm 9.7 (57-89)	79 \pm 6.5 (67-91)	75 \pm 9.2 (60-92)	64 \pm 16 (43-96)
SO_2 ($\mu\text{g m}^{-3}$)	1.7 \pm 1.2 (0.5-4)	0.9 \pm 0.74 (0.21-2.8)	3.1 \pm 2 (0.58-6.5)	6.7 \pm 3.9 (0.42-14)
NO_2 ($\mu\text{g m}^{-3}$)	4.2 \pm 2.1 (1.8-9.1)	1.7 \pm 1.3 (0.31-4.5)	4 \pm 1.9 (1.1-8.2)	6.2 \pm 2.3 (1.5-10)
CO (mg m^{-3})	0.42 \pm 0.07 (0.31-0.55)	0.27 \pm 0.08 (0.18-0.45)	0.43 \pm 0.09 (0.27-0.58)	0.46 \pm 0.07 (0.36-0.58)
O_3 ($\mu\text{g m}^{-3}$)	104 \pm 12 (89-121)	82 \pm 25 (62-142)	93 \pm 20 (68-127)	83 \pm 20 (34-109)
OC ($\mu\text{g m}^{-3}$)	2.2 \pm 1.2 (0.98-4.7)	1.6 \pm 0.86 (0.49-3.7)	3.1 \pm 1.5 (0.84-6.1)	4.6 \pm 1.9 (0.91-7.3)
EC ($\mu\text{g m}^{-3}$)	0.51 \pm 0.11 (0.35-0.68)	0.48 \pm 0.20 (0.15-0.83)	0.56 \pm 0.15 (0.29-0.78)	0.69 \pm 0.13 (0.43-0.89)
Inorganic components (ng m^{-3})				
SO_4^{2-}	6.2 \pm 2.2 (2.6-9.8)	5.0 \pm 3.9 (1.2-15)	7.6 \pm 2.9 (2.8-11)	6.3 \pm 3.0 (1.1-13)
NO_3^-	0.06 \pm 0.11 (NA ^a -0.39)	0.01 \pm 0.02 (0.002-0.06)	0.19 \pm 0.39 (0.008-1.5)	1.3 \pm 1.1 (0.07-4.2)
NH_4^+	1.7 \pm 0.55 (0.75-2.3)	1.4 \pm 1.2 (0.3-4.5)	2.3 \pm 0.99 (0.72-3.8)	2.2 \pm 1.2 (0.36-5.1)
K^+	0.21 \pm 0.1 (0.08-0.42)	0.13 \pm 0.14 (0.03-0.46)	0.28 \pm 0.15 (0.06-0.49)	0.39 \pm 0.15 (0.08-0.59)
Nitrated aromatic compounds (ng m^{-3})				
4-nitrophenol (4NP)	0.18 \pm 0.13 (0.04-0.49)	0.05 \pm 0.04 (0.01-0.16)	0.32 \pm 0.28 (0.04-1.1)	0.74 \pm 0.34 (0.14-1.3)
3-methyl-4-nitrophenol (3M4NP)	0.03 \pm 0.03 (0.01-0.09)	0.05 \pm 0.02 (0.03-0.08)	0.04 \pm 0.02 (0.02-0.09)	0.06 \pm 0.04 (0.01-0.12)
2,4-dinitrophenol (2,4-DNP)	0.06 \pm 0.03 (0.03-0.13)	0.06 \pm 0.03 (0.03-0.14)	0.08 \pm 0.03 (0.03-0.14)	0.09 \pm 0.05 (0.03-0.18)
4-nitroguaiacol (4NGA)	0.07 \pm 0.03 (0.03-0.10)	0.07 \pm 0.03 (0.03-0.14)	0.07 \pm 0.03 (0.02-0.14)	0.05 \pm 0.02 (0.03-0.09)
5-nitroguaiacol (5NGA)	0.21 \pm 0.10 (0.06-0.37)	0.29 \pm 0.13 (0.07-0.48)	0.32 \pm 0.11 (0.11-0.51)	0.22 \pm 0.1 (0.07-0.42)
4-nitrocatechol (4NC)	0.34 \pm 0.31 (0.07-1.1)	0.14 \pm 0.07 (0.03-0.27)	0.64 \pm 0.48 (0.13-1.7)	1.6 \pm 0.87 (0.27-3.0)

4-methyl-5-nitrocatechol (4M5NC)	0.20±0.08 (0.09-0.33)	0.19±0.06 (0.11-0.31)	0.34±0.1 (0.2-0.53)	0.39±0.19 (0.1-0.73)
3-nitrosalicylic acid (3NSA)	0.07±0.05 (0.03-0.2)	0.04±0.02 (0.01-0.08)	0.09±0.04 (0.04-0.18)	0.19±0.08 (0.04-0.31)
3-nitrosalicylic acid (5NSA)	0.12±0.10 (0.04-0.39)	0.07±0.04 (0.02-0.17)	0.23±0.13 (0.08-0.53)	0.55±0.29 (0.08-1.1)
NACs	1.3±0.75 (0.52-3.1)	0.97±0.36 (0.34-1.7)	2.1±0.94 (0.72-4.0)	3.9±1.5 (1.3-6.3)
Other organic components (ng m⁻³)				
Fossil fuel <i>n</i> -alkanes (ff- <i>n</i> -alkanes)	6.3±3.1 (2.7-12)	3.2±1.3 (1.5-6.1)	9.3±4.7 (3.9-20)	18±5.6 (5.7-28)
PAHs	1.5±0.86 (0.59-3.1)	0.54±0.30 (0.23-1.3)	2.1±1.1 (0.68-4.2)	4.5±1.8 (1.2-6.5)
Levoglucozan	15±17 (3.8-62)	4.2±1.7 (1.3-7.5)	23±13 (5.7-41)	52±21 (20-86)
Trehalose	0.63±0.25 (0.29-1.1)	0.87±0.41 (0.25-1.5)	0.49±0.33 (0.23-1.3)	0.36±0.14 (0.12-0.65)

^a NA: not available.

^b The numbers in the first line indicate mean ± std, and the numbers in the second line indicate lowest value-highest value.

219 3.2 Abundance and seasonal variations of NACs

220 Table 1 lists the measured concentrations of the major PM_{2.5} constituents, and
221 Fig.2 shows the seasonal fluctuations of the nine NACs throughout the year. Nine
222 different NACs' average concentrations varied significantly throughout the year, with
223 winter having the greatest levels (3.9± 1.5 ng m⁻³), followed by autumn (2.1± 0.94 ng
224 m⁻³), spring (1.3± 0.75 ng m⁻³), and summer (0.97± 0.36 ng m⁻³). The total NACs
225 concentrations in the current and earlier works have been compared in Table 2. The
226 total NACs concentration in this study was significantly lower in comparison to that
227 predicted for urban sites in China, particularly in winter and autumn, such as in Beijing
228 (20± 12 ng m⁻³ in autumn, 74± 51 ng m⁻³ in winter) (Li et al., 2020c), Jinan (9.8± 4.2
229 ng m⁻³ in autumn, 48± 26 ng m⁻³ in winter) (Wang et al., 2018), Xi'an (17± 12 ng m⁻³

230 in winter) (Wu et al., 2020), and Hong Kong ($12 \pm 14 \text{ ng m}^{-3}$ in winter) (Chow et al.,
231 2015). The main reason was that there are more pollutant emissions in and around
232 urbans with the high levels of precursors and oxidants. Moreover, as compared to the
233 levels in rural and background sites during summertime in China, the levels in this work
234 were also much lower, for instance, Wangdu (Wang et al., 2018), Yucheng, (Wang et al.,
235 2018), Mt.Tai (Wang et al., 2018), and Xianghe (Teich et al., 2017). The anthropogenic
236 pollutants (e.g. SO_2 , NO_2 , CO) were typically lower in summer, indicating the air at the
237 time of sampling was relatively clean in this work. While at above mentioned rural and
238 background sites, the atmospheric environment in summer is often affected by
239 surrounding pollution sources (e.g. coal combustion from nearby industries) (Wang et
240 al., 2018). In comparison with the studies abroad, the total NAC concentrations in this
241 investigation were also comparatively lower than the measurements in winter, such as
242 in the Detling, UK (Mohr et al., 2013), TROPOS institute and the Melpitz research site,
243 Germany (Teich et al., 2017), Ljubljana, Slovenia (Kitanovski et al., 2012) and Hamme,
244 Belgium (Kahnt et al., 2013), where NACs measured all had a significant contribution
245 from biomass burning during the sampling time.

Table 2. Measured concentrations of nitrated aromatic compounds in domestic and foreign researches over the last decade.

Sampling site	Sampling period	Aerosol Type	NAC Species ^a	Concentrations (ng m ⁻³)	References
Mt. Wuyi, China	Spring, 2014	PM _{2.5}		1.3 ± 0.75	This study
	Summer, 2014		①②③④⑤⑥	0.97 ± 0.36	
	Autumn, 2014		⑦⑧⑨	2.1 ± 0.94	
	Winter, 2014-2015			3.9 ± 1.5	
Beijing, China	Apr., 2017	PM _{2.5}	①②③④⑤⑥	8.6 ± 6.7	Ren et al., 2022
	Jul., 2017		⑦⑧⑨	8.5 ± 3.9	
Beijing, China	Sep. -Nov., 2017	PM _{2.5}	①②③④⑥⑦	20 ± 12	Li et al., 2020
	Dec., 2017-Feb., 2018		⑧⑨	74 ± 51	
Dezhou, China	Nov. 2017-Jan. 2018	PM _{2.5}	①②③④⑤⑥ ⑦⑧⑨⑩ ⑪⑫⑬⑭⑮	299	Salvador et al., 2020
Beijing, China	May-Jun., 2016	PM _{2.5}	①②⑥⑦⑩ ⑪⑫⑬	6.6	Wang et al., 2019
Xi'an, China	Jan., 2017	PM _{2.5}	①②③④⑤⑥	17 ± 12	Wu et al., 2020
	Jul.-Aug., 2017		⑦⑧⑨	0.40 ± 0.27	
Jinan, China	Nov. 2013-Jan., 2014			48 ± 26	
Yucheng, China	Sep., 2014	PM _{2.5}	①②⑥⑦⑧⑨	9.8 ± 4.2	Wang et al., 2018
	Jun., 2014		⑩⑪⑫	5.7 ± 2.8	
Wangdu, China	Jun., 2014			5.9 ± 3.8	
Mt. Tai, China	Jul.-Aug., 2014			2.5 ± 1.6	
Wangdu, China	Jun., 2014	PM ₁₀	①②③⑧⑨⑩	9.2	Teich et al., 2017
Xianghe, China	Jul.-Aug., 2013		⑬⑭	3.6	
Hong Kong, China	Spring, 2010-2012	PM _{2.5}		2.7 ± 3.6	Chow et al., 2015
	Summer, 2010-2012		①②⑥⑦⑩	2.2 ± 4.9	
	Autumn, 2010-2012		⑪⑫⑬	6.5 ± 6.9	
	Winter, 2009-2012			12 ± 14	
TROPOS, Germany	Jan.-Feb., 2014	PM ₁₀	①②②③⑧⑨	16	Teich et al., 2017
Melpitz, Germany	Jan.-Feb., 2014		⑩⑬⑭	12	
Waldstein, Germany	Jul., 2014		⑧⑨	0.3	
	Jul., 2014			0.4	
Port Angeles, WA	Jan.21-Mar.6. 2014	PM _{2.5}	①③④⑤⑥⑦ ⑮	92	Gaston et al., 2016
Detling, UK	Jan.-Feb., 2012	PM ₁	①③⑥⑦⑮	19	Mohr et al., 2013
Hamme, Flanders, Belgium	Spring, 2010	PM ₁₀		3.8	Kahnt et al., 2013
	Summer, 2010		①⑥⑦	2.2	
	Autumn, 2010		⑪⑫⑬	13	
	Winter, 2010			32	

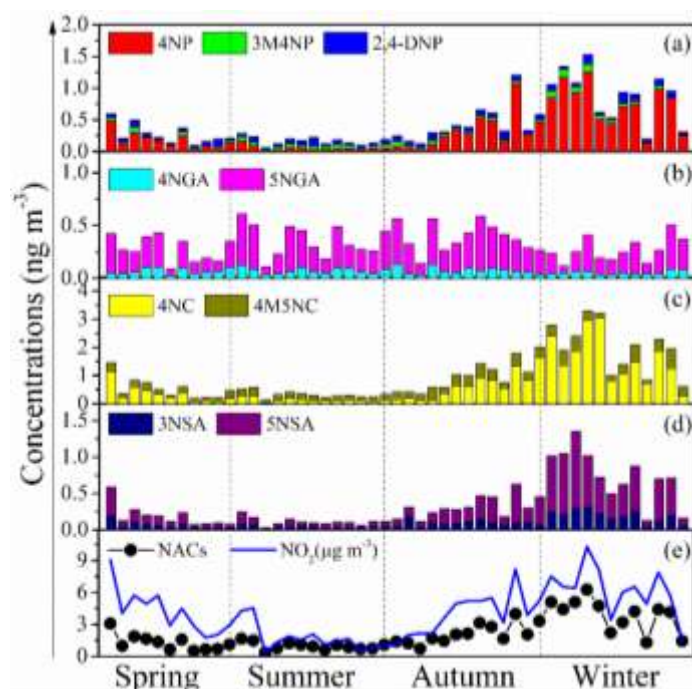
Ljubljana, Slovenia	Dec., 2010-Jan., 2011 Aug., 2010	PM ₁₀	①②③④⑤⑥ ⑦⑧⑨⑩ ⑪⑫	150 0.9	Kitanovski et al., 2012
------------------------	-------------------------------------	------------------	----------------------	------------	----------------------------

^a ①4-nitrophenol ②3-methyl-4-nitrophenol ③2,4-dinitrophenol ④4-nitroguaiacol ⑤5-nitroguaiacol
⑥4-nitrocatechol ⑦4-methyl-5-nitrocatechol ⑧3-nitro-salicylic acid ⑨5-nitro-salicylic acid ⑩2-
methyl-4-nitrophenol ⑪3-methyl-5-nitrocatechol ⑫3-methyl-6-nitrocatechol ⑬2,6-dimethyl-4-
nitrophenol ⑭3,4-dinitrophenol ⑮4-methyl-2-nitrophenol

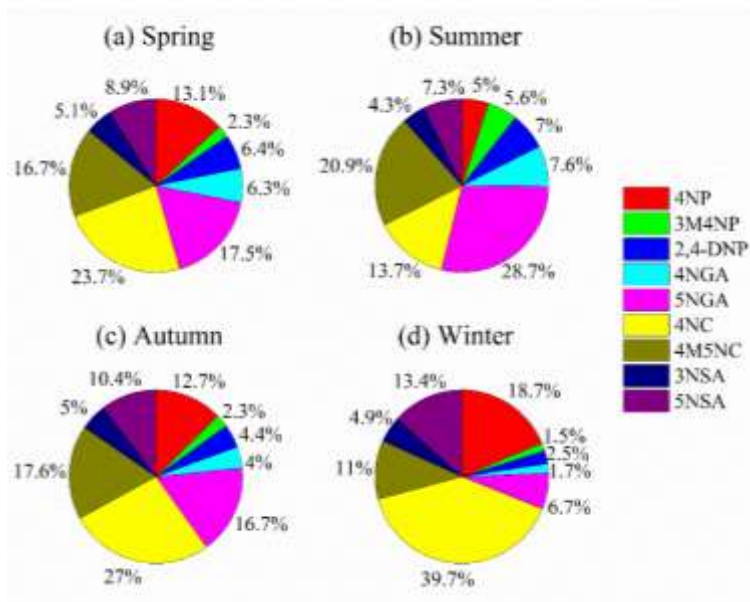
246 For each NAC species, NPs (including 4NP, 3M4NP, 2, 4-DNP) (Fig. 2a), NCs
247 (including 4NC, 4M5NC) (Fig. 2c), and NSAs (including 3NSA, 5NSA) (Fig. 2d) have
248 the same seasonal trends as the total NACs, with characteristics of higher
249 concentrations in winter than in other seasons. It should be noted that some NP species,
250 such as 2,4-DNP, did not have a distinct seasonal variation mainly due to the different
251 generation mechanisms. Our previous work has shown that 2,4-DNP were primarily
252 produced by secondary formation with aqueous-phase oxidation as the major route of
253 production (Ren et al., 2022), consisting with other researches (Cheng et al., 2021).
254 However, on the contrary, there were no obvious seasonal trends for NGAs (including
255 4NAG and 5NGA) (Fig. 2b). Averagely, 4NC was the most abundant species
256 throughout the year (25.8%), followed by 5NGA (17.6%) (Fig. S1), with different
257 proportions of molecular composition in different seasons (Fig. 3). 4NC was the only
258 NACs species that accounted for more than 20% in spring (23.7%), autumn (27%), and
259 winter (39.7%). The most prevalent compound over the summer was 5NGA (28.7%),
260 followed by 4M5NC (20.9%). These findings contrasted with those of earlier studies
261 on urban areas, which often revealed that 4NP had the greatest levels, followed by 4NC
262 (Li et al., 2020c; Wang et al., 2018; Wang et al., 2019).

263 As mentioned above, obvious seasonal variations were observed in the
264 concentrations and compositions of NACs in Mt. Wuyi. The following sections

265 comprise the implied differences in the primary sources and the secondary formation
 266 pathways.



267
 268 Fig.2 Temporal variations of each NACs species (4NP: 4-nitrophenol; 3M4NP: 3-
 269 methyl-4-nitrophenol; 2,4-DNP: 2,4-dinitrophenol; 4NGA: 4-nitroguaiacol; 5NGA: 5-
 270 nitroguaiacol; 4NC: 4-nitrocatechol; 4M5NC: 4-methyl-5-nitrocatechol; 3NSA: 3-
 271 nitrosalicylic acid; 5NSA: 5-nitrosalicylic acid).



272
 273 Fig.3 Relative contribution of each NACs species during the sampling time (4NP: 4-
 274 nitrophenol; 3M4NP: 3-methyl-4-nitrophenol; 2,4-DNP: 2,4-dinitrophenol; 4NGA: 4-
 275 nitroguaiacol; 5NGA: 5-nitroguaiacol; 4NC: 4-nitrocatechol; 4M5NC: 4-methyl-5-
 276 nitrocatechol; 3NSA: 3-nitrosalicylic acid; 5NSA: 5-nitrosalicylic acid).

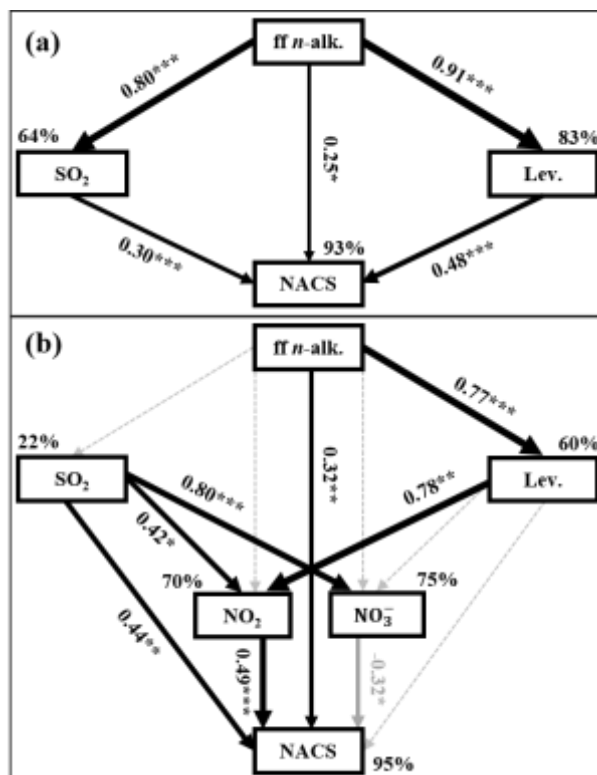
277 **3.3 Source apportionment**

278 **3.3.1 Source identification**

279 For further clarification regarding the influencing factors and sources of NACs,
280 the **relationship** between total and individual NAC species and the related pollutants
281 were analyzed based on the results of Pearson correlations depicted in Table 3 (for the
282 whole campaign) and Tables S3-6 (for the four seasons), including PM_{2.5}, SO₂, NO₂,
283 O₃, and other chemical components. It is noteworthy that total NACs and all identified
284 NACs species manifested strong correlations with PM_{2.5} in the whole year, indicating
285 that they are important components of PM_{2.5}. There were good relationships between
286 NACs and primary pollutants in the whole year, such as SO₂ ($r=0.859$, $p<0.01$), ff-*n*-
287 alkanes ($r=0.927$, $p<0.01$), PAHs ($r=0.927$, $p<0.01$), levoglucosan ($r=0.931$, $p<0.01$),
288 and K⁺ (i.e., a BB tracer, $r=0.817$, $p<0.01$) (Table 3). Furthermore, the model calculation
289 results of SEM indicated ff-*n*-alkanes, SO₂, and levoglucosan would account for 93%
290 of NACs (Fig. 4a). All of these connections indicated that burning emissions throughout
291 the year, such as the burning of coal (Lu et al., 2019b), biomass (Wang et al., 2017; Lin
292 et al., 2017; Chow et al., 2015), and burning of petroleum (Lu et al., 2019a), had a
293 substantial impact on NACs.

294 Additionally, total NACs also showed strong correlations with NO₂ ($r=0.862$,
295 $p<0.01$), SO₄²⁻ ($r=0.396$, $p<0.01$), NO₃⁻ ($r=0.757$, $p<0.01$), NH₄⁺ ($r=0.524$, $p<0.01$),
296 probably suggesting that the secondary formation of NACs was also important in the
297 campaign. Here, the NACs concentration was strongly associated with NO₂, especially
298 in the winter (Fig. 2e, Fig. 4b), and correlated better than other secondary tracers (Table

299 3), suggesting that NO₂ is a relatively importance component in the creation of NACs.



300
 301 Fig. 4 Structural equation model (SEM) demonstrating the effects of ff *n*-alk., SO₂, Lev.
 302 and NO₂ on annual (a) or winter (b) mean NACs. Black solid arrows indicate
 303 significant positive relationships, gray solid arrows indicate significant negative
 304 relationships and black dashed arrows indicate nonsignificant path coefficients.
 305 The width of arrows is proportional to the strength of path coefficients. Numbers
 306 on arrows are standardized path coefficients (equivalent to correlation
 307 coefficients), asterisks following the numbers imply significant relationships (**p*
 308 < 0.05, ***p* < 0.01, ****p* < 0.001). Percentages (R²) close to endogenous
 309 variables indicate the variance explained by the ff *n*-alk., SO₂, Lev. and NO₂.

Table 3. Pearson correlations between individual NAC species and meteorological parameters, aerosol components, and gas pollutants during the whole campaign (n = 49).

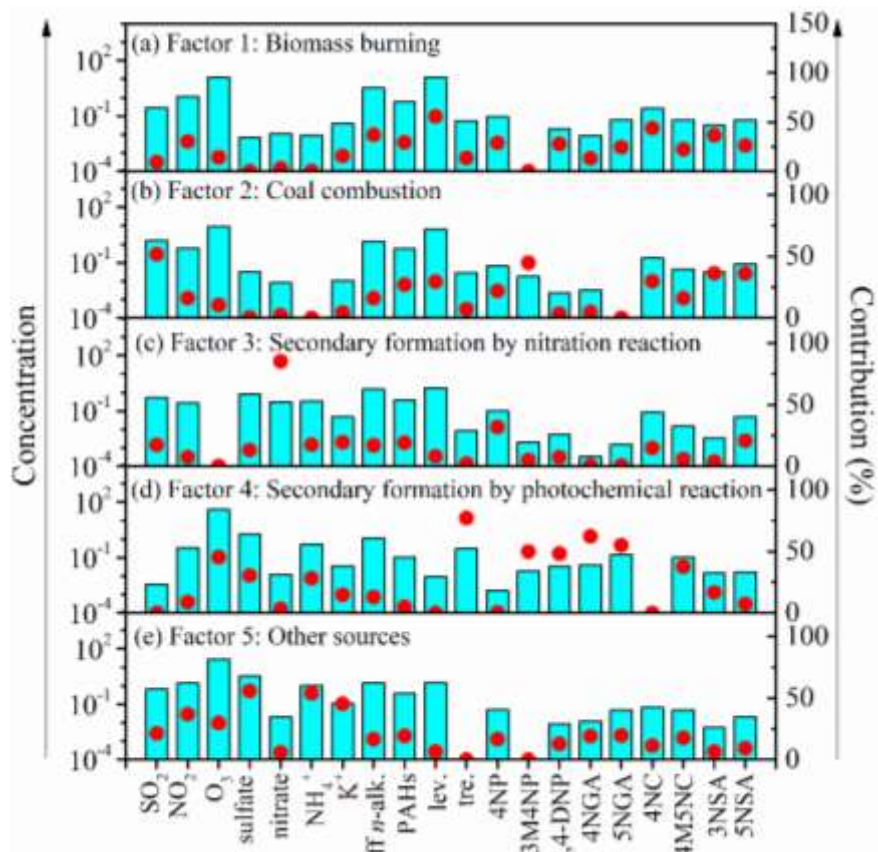
	NACs	4NP	3M4NP	2,4-DNP	4NGA	5NGA	4NC	4M5NC	3NSA	5NSA
PM _{2.5}	0.657**	0.649**	0.376**	0.359*	0.308*	0.521**	0.501**	0.703**	0.561**	0.564**
SO ₂	0.859**	0.887**	0.520**	0.299*	-0.184	-0.053	0.781**	0.637**	0.748**	0.889**
NO ₂	0.862**	0.834**	0.329*	0.347*	-0.142	0.103	0.845**	0.543**	0.762**	0.774**
O ₃	0.146	0.145	0.028	0.024	0.308*	0.403**	0.029	0.348*	0.174	0.102
ff- <i>n</i> -alkanes	0.927**	0.942**	0.364*	0.475**	-0.140	0.090	0.841**	0.732**	0.834**	0.880**
PAHs	0.927**	0.944**	0.486**	0.347*	-0.205	-0.049	0.857**	0.661**	0.838**	0.942**
Levoglucosan	0.931**	0.885**	0.299*	0.392**	-0.207	0.113	0.884**	0.721**	0.881**	0.860**
K ⁺	0.817**	0.805**	0.308*	0.363*	0.109	0.330*	0.707**	0.736**	0.709**	0.732**
SO ₄ ²⁻	0.396**	0.412**	0.281	0.285*	0.411**	0.516**	0.250	0.502**	0.272	0.305*
NO ₃ ⁻	0.757**	0.829**	0.448**	0.322*	-0.225	-0.108	0.701**	0.486**	0.618**	0.766**
NH ₄ ⁺	0.524**	0.560**	0.314*	0.321*	0.276	0.443**	0.385**	0.547**	0.373**	0.442**

**Significant correlation at the 0.01 level.

*Significant correlation at the 0.05 level.

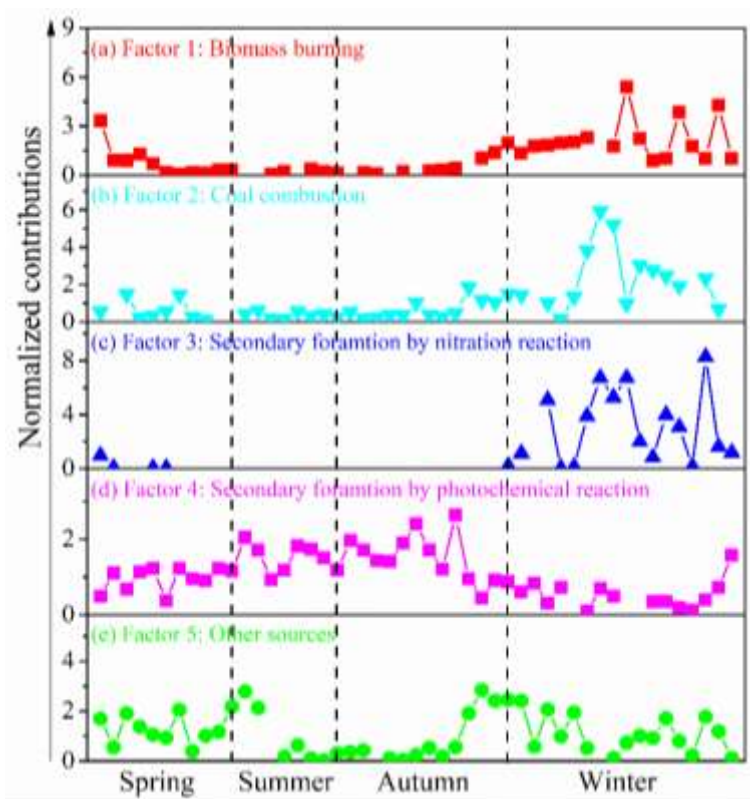
310 To further quantitatively the effects of various pollutants emissions on NACs
311 during the campaign, this work identified five sources with applying the PMF model.
312 These sources have been shown in Fig. 5 and Fig. 6. The first source factor, biomass
313 burning, was identified that levoglucosan loading was larger in this component profile
314 than in others. Furthermore, there were also with other high loading anthropogenic
315 primary organic markers, included ff-*n*-alkanes, PAHs, SO₂, and NO₂ (Fig. 5a). This
316 sources had obviously seasonal variation characteristics with much more intense in
317 winter and early spring than in other seasons (Fig. 6a). It contributed 18.3% of the total
318 particulate NACs at the summit of Mt. Wuyi during the whole campaign (Fig. 7a).
319 Based on the air mass backward trajectories, it was assumed to originate from the long-
320 range transport (Fig. 1). Coal combustion was identified the second source factor, with
321 high levels of SO₂ (Fig. 5b). This source was also much more intense in winter than in
322 other seasons and affected by the transport of pollutants. (Fig. 6b). It contributed 16.5%

323 of the total particulate NACs at the summit of Mt. Wuyi during the whole campaign
324 (Fig. 7a). The third source factor namely secondary formation by nitration reaction
325 showed high concentrations of NO_3^- (Fig. 5c). This source was much more intense in
326 winter than in other seasons (Fig. 6c). It contributed 10.3% of the total particulate NACs
327 at the summit of Mt. Wuyi during the whole campaign (Fig. 7a). And this source may
328 be mainly affected by the transport of pollutants. Secondary formation by
329 photochemical reaction were recognized as the fourth source factor, with relatively high
330 levels of O_3 and low levels of anthropogenic pollutants (e.g. SO_2 , NO_2 , ff-*n*-alkanes,
331 PAHs, levoglucosan), indicating it mostly a local source (Fig. 5d). It is noteworthy that
332 trehalose also showed relatively high levels because this component is a naturally
333 existing carbohydrate in vegetations, which were abundant in the sampling site.
334 Different from the mentioned above sources, contributions from this source was
335 averagely higher in summer than in other seasons (Fig. 6d). It contributed 33% of the
336 total particulate NACs at the summit of Mt. Wuyi during the whole campaign (Fig. 7a).
337 Other sources was identified as the last factor including primary emissions and
338 secondary formation (Fig. 5e), due to with the highest loading of SO_2 , NO_2 and K^+ as
339 well as O_3 , SO_4^{2-} and NH_4^+ . The contribution of this source was more significant in
340 spring and later autumn, with the least amount in later summer and early autumn (Fig.
341 6e). Based on these variations of markers, this source was influenced by both transport
342 and local pollutants. It contributed 21.9% of the total particulate NACs at the summit
343 of Mt. Wuyi during the whole campaign year (Fig. 7a).



344
 345
 346

Fig.5 Source profiles of NACs obtained from PMF analysis (ff *n*-alk.: ff *n*-alkane. lev.: levoglucosan. tre.: trehalose).



347
 348

Fig. 6 Time variations of normalized contributions of each source.

3.3.2 Contributions of each source in different seasons

As mentioned above, those five sources had obviously different seasonal variation characteristics. Fig.7 compared the average contributions of the five source factors to the concentrations of total particulate NACs at the summit of Mt. Wuyi. This clarifies the difference in the sources of them in the four seasons at mountain background station of Southeast China.

During springtime, other sources had the biggest influence on NACs, followed by secondary formation by photochemical reaction, which accounted respectively for 37.1% and 31.3% of the total (Fig. 7b). For total NACs, the correlation coefficient (Pearson r) was strong with SO_2 , n -alkanes, PAHs, levoglucosan, and K^+ ($r > 0.73$, $p < 0.01$), and the total NACs correlated well with NO_2 , O_3 , NO_3^- , and NH_4^+ ($r > 0.70$, $p < 0.01$) (Table S3). The outcome indicated that NACs originate not only from primary emissions but also from the secondary formation. Furthermore, The Pearson r for levoglucosan ($r = 0.933$, $p < 0.01$) and NO_2 ($r = 0.945$, $p < 0.01$) were higher in comparison to other parameters, suggesting that the biomass burning and NO_2 had significant effects on NACs at the summit of Mt. Wuyi in spring.

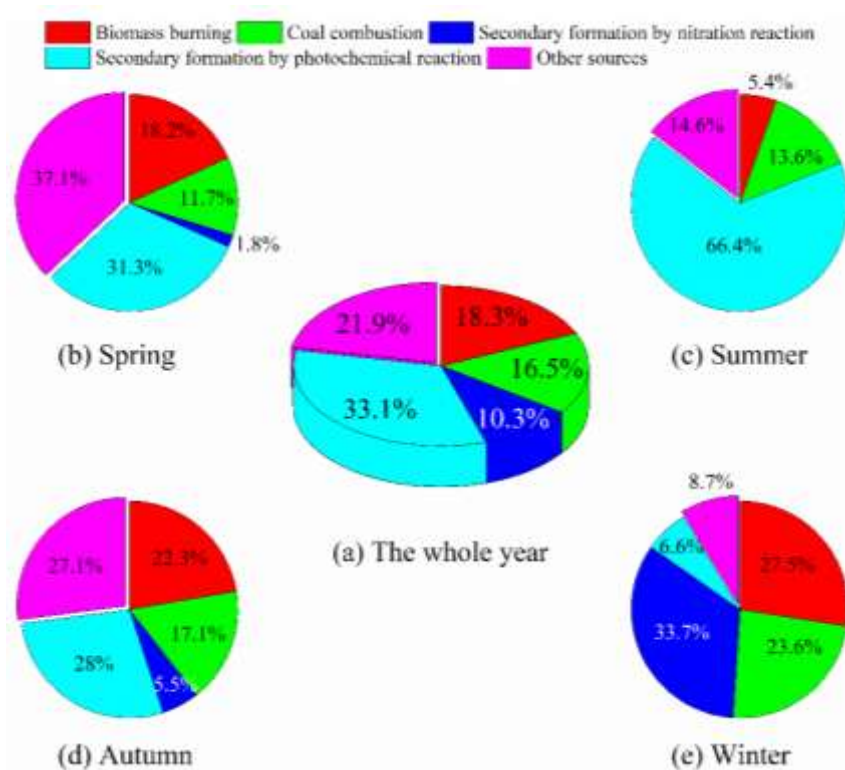
During summertime, secondary formation by photochemical reaction were the largest contributors to NACs, with the relative contributions accounting for more than 65% of the total (Fig. 7c). The photochemical production of NACs is related to the oxidation of aromatics in the presence of NO_2 , including the $\cdot\text{OH}$ oxidation and the $\text{NO}_3\cdot$ oxidation (Cai et al., 2022; Ren et al., 2022; Yi Chen et al., 2022; Finewax et al., 2018). The correlation coefficient (Pearson r) of total NACs was strong with NO_2

371 ($r=0.869$, $p<0.01$), O_3 ($r=0.786$, $p<0.01$), SO_4^{2-} ($r=0.884$, $p<0.01$), NO_3^- ($r=0.678$,
372 $p<0.05$), and NH_4^+ ($r=0.881$, $p<0.01$) (Table S4), suggesting that the secondary
373 formation contributes significantly to the summertime NACs at the summit of Mt. Wuyi.
374 And the strong associations between O_3 and NACs further support the significance of
375 photochemical oxidation for NACs. The secondary formation has been identified as a
376 major cause of the origin of atmospheric nitrated phenols, particularly in the summer,
377 during the various field and modeling investigations conducted recently (Yuan et al.,
378 2016; Mayorga et al., 2021; Xie et al., 2017; Cai et al., 2022; Wang et al., 2019).

379 During autumn, the relative contributions of each source of NACs were similar to
380 those observed in spring. Secondary formation by photochemical reaction and other
381 sources made almost equal contributions to NACs, which accounted for 28% and 27.1%,
382 respectively (Fig. 7d). Biomass burning also made a relatively large contribution to
383 NACs (22.3%). There was still a strong correlation between NACs and NO_2 ($r=0.886$,
384 $p<0.01$). It is noteworthy that the correlation coefficient (Pearson r) of total NACs was
385 stronger with SO_2 ($r=0.805$, $p<0.01$) and SO_4^{2-} ($r=0.615$, $p<0.05$), and weaker with O_3
386 ($r=0.165$) in autumn than with the same in spring (Table S5). The findings revealed that
387 at the summit of Mt. Wuyi in autumn, the proportional contribution of coal combustion
388 was rising and the impact of photochemical reaction was declining.

389 During wintertime, secondary formation by nitration reaction was the largest
390 contributor for NACs (33.7%), followed by biomass burning (27.5%) and coal
391 combustion (23.6%) (Fig. 7e). The total NACs correlated better with NO_2 ($r=0.879$,
392 $p<0.01$) than any other parameters (Table S6), thereby pointing towards significant

393 involvement of NO₂ in NACs formation. According to earlier research, coal combustion
 394 and biomass burning had a greater contribution to NACs in the winter (Cai et al., 2022),
 395 with direct emissions from biomass burning in the range of 0.4 to 11.1 mg kg⁻¹ (Iinuma
 396 et al., 2007; Wang et al., 2017). Furthermore, earlier research suggested that the
 397 detection of increased amounts of particulate phenols could be significantly attributed
 398 to coal combustion activities. The emission factors ranged from 0.2 to 10.1 mg kg⁻¹ for
 399 bituminite, anthracite, lignite chunks, and briquettes. The residential coal combustion
 400 resulted in a net emission of 178 ± 42 Mg of fine particles of nitrated phenols, according
 401 to statistics of domestic coal consumption in a total of 30 provinces in Chinese in 2016
 402 (Lu et al., 2019b).



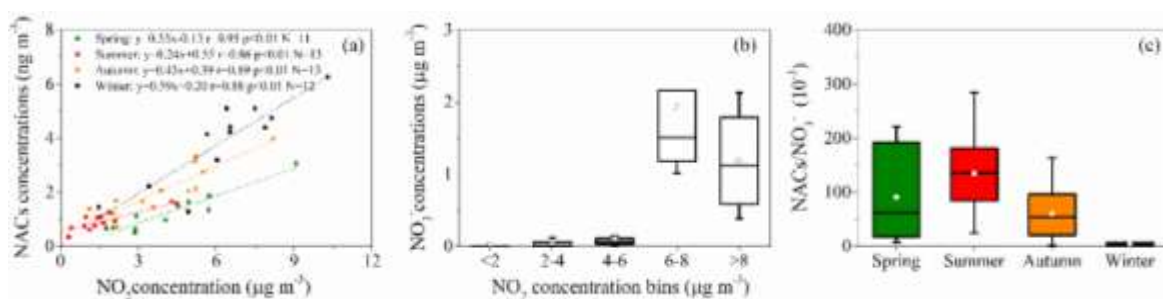
403
 404

Fig. 7 Relative contributions of each source for NACs in different seasons.

405 3.4 Impact of NO₂ on NACs

406 The total measured NACs and NO₂ in our study displayed comparable temporal
407 fluctuations (Fig. 2e), and they revealed strong correlations in the course of the entire
408 campaign ($r=0.879$, $p<0.01$). To examine the impact of NO₂ abundance further on the
409 second generation of NACs and the current form, concentrations of total NACs and
410 nitrate (NO₃⁻) as a function of NO₂ abundance, and the fluctuations of [NACs] / [NO₃⁻]
411 mass ratios were plotted in Fig. 8. Generally, with increasing NO₂ abundance, the
412 concentrations of NACs and NO₃⁻ showed higher (Fig. 8a, b), consisting with earlier
413 investigations (Cai et al., 2022; Wang et al., 2018; Ren et al., 2022). It was worth noting
414 that the encouraging effect of NO₂ was more pronounced in winter than in other seasons
415 (Fig. 8a). This perhaps because winter had much higher NO_x abundance with higher
416 VOC precursor oxidation capacity (Cai et al., 2022). Moreover, the results of SEM also
417 had proved this point. The influence of the weight of NO₂ on NACs was significantly
418 greater than that of other factors in winter, such as *n*-alkane and SO₂, although they
419 all had significant effects on NACs (Fig. 4b). Fig. 8c showed the variations of [NACs]
420 / [NO₃⁻] mass ratios in different seasons. In general, the mass ratios ranged from 1 to
421 285 (ng/μg) with average of 73 (ng/μg) during the whole campaign. In previous studies,
422 this ratio was generally between 1 (ng/μg) and 14 (ng/μg) at urban stations. For example,
423 it was averaged 13.5 (ng/μg) in Beijing during spring and summer (Ren et al., 2022),
424 1.4 (ng/μg) and 2.1 (ng/μg) in Jinan during summer and winter, respectively (Wang et
425 al., 2018), and from 1 to 9 (ng/μg) in Shanghai (Cai et al., 2022). This mass ratio was
426 obviously much higher in comparison to that observed in urban sites, and this

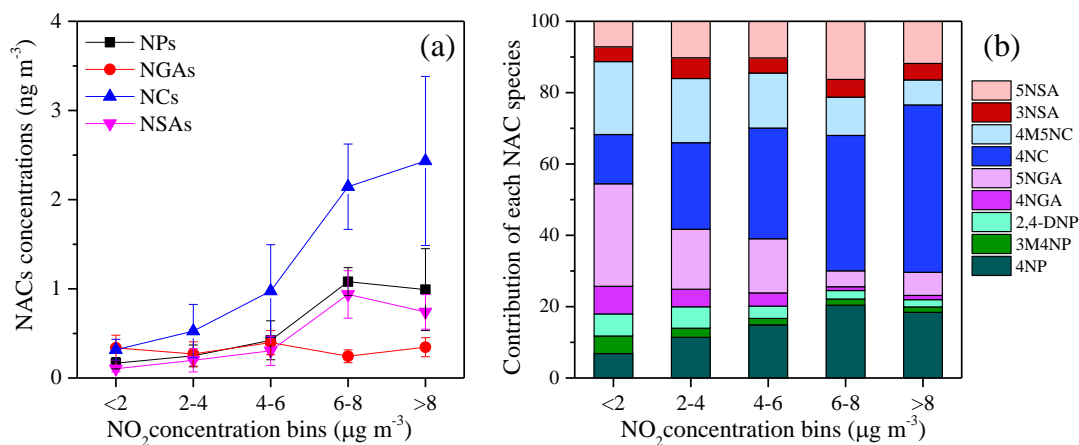
427 phenomenon would suggest that NACs were more likely generated in the background
 428 site at low NO_x levels. According to certain studies conducted in urban centers, when
 429 NO_2 levels were high ($\text{NO}_2 > 30 \text{ ppb}$), the NO_2 excess would be further oxidized to
 430 generate inorganic nitrate, which would lead to a change in the relative dominance of
 431 organic and inorganic compounds. When NO_2 was scarcer, a higher portion of NO_2 was
 432 covered into organic nitrogen (Cai et al., 2022; Wang et al., 2018). The NO_2 levels on
 433 submit of Mt. Wuyi were much lower than those in the urban's atmosphere. Moreover,
 434 the ratio of $[\text{NACs}] / [\text{NO}_3^-]$ highest with lowest NO_2 levels in summer than in other
 435 three seasons (Fig. 8c). These results further indicated that the formation of organic
 436 nitrated aerosols was relatively sensitive to NO_2 at the low- NO_x level. In addition, the
 437 possible reason for the low level of $[\text{NACs}] / [\text{NO}_3^-]$ in winter was that NO_3^- was an
 438 increasingly important component of $\text{PM}_{2.5}$ especially during heavy pollution (Wang et
 439 al., 2023; Fu et al., 2020).



440
 441 Fig. 8 Concentrations of NACs (a), nitrate (NO_3^-) (b) as a function of NO_2
 442 concentration bins, and NACs / NO_3^- ratios (c) during the whole sampling time. The
 443 mean values are represented by the markers and the 25th and 75th percentiles are
 444 represented by whiskers.

445 To investigate the influence of NO_2 on NAC compositions, the variation of NAC
 446 compositions as a function of NO_2 levels was shown in Fig. 9. In this work, NO_2 levels
 447 had impact on NAC composition besides of encouraging the synthesis of them,

448 especially for NCs (Fig. 9a). The contributions of 4NC for total NACs was significantly
 449 at elevated NO₂ levels. When NO₂ reached above 8 μg m⁻³, the concentrations of NACs
 450 reached their maximum values and 4NC made the greatest contribution to the total
 451 NACs followed by 4NP at this time (Fig. 9b). The role of elevated NO₂ in promoting
 452 formation of NCs was more obvious than NPs, mainly because of their difference in
 453 generation mechanism. The major formation pathway of NCs was the oxidation of
 454 aromatics in the presence of NO₂ (Wang et al., 2019; Xie et al., 2017). While NPs could
 455 originate through gas-phase oxidation of phenol, benzene, and toluene by OH or NO₃
 456 radicals in the presence of NO₂, and particle-phase NPs were strongly dependent on the
 457 gas-to-particle partitioning and gas-phase loss (Wang et al., 2019; Ji et al., 2017; Yuan
 458 et al., 2016).



459 Fig. 9 Concentrations of NACs (a) and (b) contribution of each NACs species as a
 460 function of NO₂ concentration bins. (NPs: 4NP, 3M4NP, and 2,4-DNP; NGAs: 4NGA
 461 and 5NGA; NCs: 4NC and 4M5NC; NSAs: 3NSA and 5NSA).

463 4 Conclusion and implications

464 NACs in fine particle were examined at the peak of Mt. Wuyi in 2014 and 2015.
 465 Nine quantified NACs manifested a significant rise in overall abundance in the winter

466 and autumn, partly as a result of air masses traveling primarily through northern heating
467 regions, and indicating strong influences of anthropogenic activities. To identify the
468 sources of NACs, the PMF receptor model was applied. There were five source factors
469 identified including biomass burning, coal combustion, secondary formation by
470 nitration reaction, secondary formation by photochemical reaction, and other sources.
471 Due to the impact of long-range transport of air pollutants, biomass burning and coal
472 combustion were important primary sources. It is important to note that secondary
473 generation was an important source of NAC in this remote areas during the sampling
474 time, and the production of organic nitrated aerosols was relatively responsive to NO₂
475 under low-NO_x conditions. This work clearly demonstrated that anthropogenic
476 emissions could impact the pollution levels and variation characteristics of NACs in the
477 atmosphere, and the crucial roles of secondary formation in the distant mountain
478 regions.

479 Previous studies had come to a consensus that organic nitrated aerosols were
480 relatively sensitive to NO₂ under low levels. However, in different atmospheric
481 conditions, different levels of NO₂ may have different effects on nitrate aerosols
482 especially at high NO_x levels. In Beijing, our prior research had shown that at NO₂
483 concentrations above 30ppb, inorganic nitrates were converted more quickly during the
484 day, while at the night, there was a shift in the corresponding products of oxidation to
485 predominantly organic ones (Ren et al., 2022). The transition from organic- to
486 inorganic-dominated products takes place in line with the switch from low- to high-
487 NO_x regimes according to Wang et al., (2019), with low-NO_x conditions being

488 predominated by organic-dominated products and a switch from majorly organic-
489 entities to inorganic ones at high-NO_x conditions (NO₂ ~ 25 ppb for the night and NO₂
490 ~20 ppb for the day). Cai et al., (2022) also indicated that inorganic nitrate
491 predominated among the NO_x oxidation products in high-NO_x concentrations
492 (NO₂>30ppb). These variations could be caused by different precursor kinds and
493 concentrations, as well as other variables. Therefore, additional and more thorough
494 research is required to fully understand the quantitative impact of NO₂ on nitrate
495 aerosols under various atmospheric conditions using laboratory simulation and field
496 measurements.

497 **Data availability**

498 The field observational and the lab experimental data used in this study are
499 available from the corresponding author upon request (Gehui Wang via
500 ghwang@geo.ecnu.edu.cn).

501 **Author contributions**

502 GW designed the research; JT and ZZ collected the samples; YR conducted the
503 experiments; YR and JW analyzed the data and wrote the paper; GW, JW and HL
504 contributed to the paper with useful scientific discussions and comments.

505 **Competing interests**

506 The authors declare that they have no conflict of interest.

507 **Acknowledgements**

508 This work is financially supported by the program from National Natural Science
509 Foundation of China (No. 41907197), the Fundamental Research Funds for Central
510 Public Welfare Scientific Research Institutes of China, Chinese Research Academy of
511 Environmental Sciences (No. 2019YSKY-018).

512

513

514 **References**

- 515 Bandowe, B. A. M., Meusel, H., Huang, R.-j., Ho, K., Cao, J., Hoffmann, T., and Wilcke, W.:
516 PM_{2.5}-bound oxygenated PAHs, nitro-PAHs and parent-PAHs from the atmosphere of a
517 Chinese megacity: seasonal variation, sources and cancer risk assessment, *Sci. Total.*
518 *Environ.*, 473, 77-87, 2014.
- 519 Berndt, T. and Bge, O.: Gas-phase reaction of OH radicals with phenol, *PCCP*, 5, 342-350,
520 <https://doi.org/10.1039/B208187C>, 2003.
- 521 Cai, D., Wang, X., George, C., Cheng, T., Herrmann, H., Li, X., and Chen, J.: Formation of
522 Secondary Nitroaromatic Compounds in Polluted Urban Environments, *J. Geophys. Res.-*
523 *Atmos.*, <https://doi.org/10.1029/2021JD036167>, 2022.
- 524 Cheng, X., Chen, Q., Li, Y., Huang, G., Liu, Y., Lu, S., Zheng, Y., Qiu, W., Lu, K., Qiu, X.,
525 Bianchi, F., Yan, C., Yuan, B., Shao, M., Wang, Z., Canagaratna, M. R., Zhu, T., Wu, Y., and
526 Zeng, L.: Secondary Production of Gaseous Nitrated Phenols in Polluted Urban
527 Environments, *Environ. Sci. Technol.*, 55, 4410-4419, 10.1021/acs.est.0c07988, 2021.
- 528 Chiapello, I., Bergametti, G., and Chaten, B.: Origins of African dusttransported over the
529 northeastern tropical Atlantic, *Journal of Geophysical Research Atmospheres*, 102, 13701-
530 13709, <https://doi.org/10.1029/97JD00259>, 1997.
- 531 Chow, K. S., Huang, X. H. H., and Yu, J. Z.: Quantification of nitroaromatic compounds in
532 atmospheric fine particulate matter in Hong Kong over 3 years: field measurement evidence

533 for secondary formation derived from biomass burning emissions, *Environmental Chemistry*,
534 13, 665, <https://doi.org/10.1071/EN15174>, 2015.

535 Comero, S., Capitani, L., and Gawlik, B.: Positive Matrix Factorisation (PMF)—An introduction
536 to the chemometric evaluation of environmental monitoring data using PMF, Office for
537 Official Publications of the European Communities, Luxembourg, 59, 2009.

538 Desyaterik, Y., Sun, Y., Shen, X., Lee, T., Wang, X., Tao, W., and Collett, J. L.: Speciation of
539 "brown" carbon in cloud water impacted by agricultural biomass burning in eastern China,
540 *Journal of Geophysical Research Atmospheres*, 118, 7389-7399,
541 <https://doi.org/10.1002/jgrd.50561>, 2013.

542 Finewax, Zachary, de, Gouw, Joost, A., Ziemann, Paul, and J.: Identification and Quantification
543 of 4-Nitrocatechol Formed from OH and NO₃ Radical-Initiated Reactions of Catechol in
544 Air in the Presence of NO_x: Implications for Secondary Organic Aerosol Formation from
545 Biomass Burning, *Environ. Sci. Technol.*, 52, 1981-1989,
546 <https://doi.org/10.1021/acs.est.7b05864>, 2018.

547 Fu, X., Wang, T., Gao, J., Wang, P., and Xue, L.: Persistent Heavy Winter Nitrate Pollution
548 Driven by Increased Photochemical Oxidants in Northern China, *Environ. Sci. Technol.*,
549 XXXX, 2020.

550 Gaston, C. J., Lopez-Hilfiker, F. D., Whybrew, L. E., Hadley, O., Mcnair, F., Gao, H., Jaffe, D.
551 A., and Thornton, J. A.: Online molecular characterization of fine particulate matter in Port
552 Angeles, WA: Evidence for a major impact from residential wood smoke, *Atmos. Environ.*,
553 138, 99-107, 2016.

554 Harrison, M. A. J., Barra, S., Borghesi, D., Vione, D., Arsene, C., and Olariu, R. I.: Nitrated
555 phenols in the atmosphere: a review, *Atmos. Environ.*, 39, 231-248,
556 <https://doi.org/10.1016/j.atmosenv.2004.09.044>, 2005.

557 Iinuma, Y., Boge, O., Graefe, R., and Herrmann, H.: Methyl-Nitrocatechols: Atmospheric
558 Tracer Compounds for Biomass Burning Secondary Organic Aerosols, *Environ. Sci.*
559 *Technol.*, 44, 8453-8459, <https://doi.org/10.1021/es102938a>, 2010.

560 Iinuma, Y., Brüggemann, E., Gnauk, T., Müller, K., Andreae, M. O., Helas, G., Parmar, R., and
561 Herrmann, H.: Source characterization of biomass burning particles: The combustion of
562 selected European conifers, African hardwood, savanna grass, and German and Indonesian
563 peat, *J. Geophys. Res.-Atmos.*, 112, D08209, <https://doi.org/10.1029/2006JD007120>, 2007.

564 Ji, Y., Zhao, J., Terazono, H., Misawa, K., and Zhang, R.: Reassessing the atmospheric
565 oxidation mechanism of toluene, *Proc Natl Acad Sci*, 114, 8169-8174, 2017.

566 Kahnt, A., Behrouzi, S., Vermeylen, R., Shalamzari, M. S., Vercauteren, J., Roekens, E., Claeys,
567 M., and Maenhaut, W.: One-year study of nitro-organic compounds and their relation to
568 wood burning in PM₁₀ aerosol from a rural site in Belgium, *Atmos. Environ.*, 81, 561-568,
569 <https://doi.org/10.1016/j.atmosenv.2013.09.041>, 2013.

570 Kitanovski, Z., Grgic, I., Vermeylen, R., Claeys, M., and Maenhaut, W.: Liquid chromatography
571 tandem mass spectrometry method for characterization of monoaromatic nitro-compounds
572 in atmospheric particulate matter, *J. Chromatogr.*, 1268, 35-43,
573 <https://doi.org/10.1016/j.chroma.2012.10.021>, 2012.

574 Kitanovski, Z., Hovorka, J., Kuta, J., Leoni, C., Proke, R., Sáníka, O., Shahpoury, P., and
575 Lammel, G.: Nitrated monoaromatic hydrocarbons (nitrophenols, nitrocatechols,
576 nitrosalicylic acids) in ambient air: levels, mass size distributions and inhalation

577 bioaccessibility, *Environmental Science and Pollution Research*, 28, 59131–59140,
578 <https://doi.org/10.1007/S11356-020-09540-3>, 2021.

579 Li, J., Wang, G., Ren, Y., Wang, J., Wu, C., Han, Y., Zhang, L., Cheng, C., and Meng, J.:
580 Identification of chemical compositions and sources of atmospheric aerosols in Xi'an, inland
581 China during two types of haze events, *Sci. Total. Environ.*, 566, 230-237, 2016.

582 Li, J., Zhang, Q., Wang, G., Li, J., Wu, C., Liu, L., Wang, J., Jiang, W., Li, L., Ho, K. F., and
583 Cao, J.: Optical properties and molecular compositions of water-soluble and water-insoluble
584 brown carbon (BrC) aerosols in Northwest China, *Atmos. Chem. Phys.*, 20, 4889–4904,
585 <https://doi.org/10.5194/acp-20-4889-2020>, 2020a.

586 Li, M., Wang, X., Lu, C., Li, R., Zhang, J., Dong, S., Yang, L., Xue, L., Chen, J., and Wang, W.:
587 Nitrate phenols and the phenolic precursors in the atmosphere in urban Jinan, China, *Sci.*
588 *Total. Environ.*, 714, <https://doi.org/10.1016/j.scitotenv.2020.136760>, 2020b.

589 Li, X., Yang, Y., Liu, S., Zhao, Q., Wang, G., and Wang, Y.: Light absorption properties of
590 brown carbon (BrC) in autumn and winter in Beijing: Composition, formation and
591 contribution of nitrated aromatic compounds, *Atmos. Environ.*, 223, 117289,
592 <https://doi.org/10.1016/j.atmosenv.2020.117289>, 2020c.

593 Liang, Y., Wang, X., Dong, S., Liu, Z., Mu, J., Lu, C., Zhang, J., Li, M., Xue, L., and Wang, W.:
594 Size distributions of nitrated phenols in winter at a coastal site in north China and the impacts
595 from primary sources and secondary formation, *Chemosphere*, 250,
596 <https://doi.org/10.1016/j.chemosphere.2020.126256>, 2020.

597 Lin, P., Bluvshstein, N., Rudich, Y., Nizkorodov, S. A., Laskin, J., and Laskin, A.: Molecular
598 Chemistry of Atmospheric Brown Carbon Inferred from a Nationwide Biomass Burning
599 Event, *Environ. Sci. Technol.*, 51, 11561-11570, <https://doi.org/10.1021/acs.est.7b02276>,
600 2017.

601 Lu, C., Wang, X., Dong, S., Zhang, J., and Wang, W.: Emissions of fine particulate nitrated
602 phenols from various on-road vehicles in China, *Environ. Res.*, 179, 108709,
603 <https://doi.org/10.1016/j.envres.2019.108709>, 2019a.

604 Lu, C., Wang, X., Li, R., Gu, R., Zhang, Y., Li, W., Gao, R., Chen, B., Xue, L., and Wang, W.:
605 Emissions of fine particulate nitrated phenols from residential coal combustion in China,
606 *Atmos. Environ.*, 203, 10-17, <https://doi.org/10.1016/j.atmosenv.2019.01.047>, 2019b.

607 Lv, S., Wang, F., Wu, C., Chen, Y., Liu, S., Zhang, S., Li, D., Du, W., Zhang, F., Wang, H.,
608 Huang, C., Fu, Q., Duan, Y., and Wang, G.: Gas-to-aerosol phase partitioning of atmospheric
609 water-soluble organic compounds at a rural site of China: An enhancing effect of NH₃ on
610 SOA formation, *Environ. Sci. Technol.*, 56, 3915–3924,
611 <https://doi.org/10.1021/acs.est.1c06855>, 2022.

612 Mayorga, R. J., Zhao, Z., and Zhang, H.: Formation of secondary organic aerosol from nitrate
613 radical oxidation of phenolic VOCs: Implications for nitration mechanisms and brown
614 carbon formation, *Atmos. Environ.*, 244, <https://doi.org/10.1016/j.atmosenv.2020.117910>,
615 2021.

616 Mohr, C., Lopez-Hilfiker, F. D., Zotter, P., A. S. H. P., Xu, L., Ng, N. L., Herndon, S. C.,
617 Williams, L. R., Franklin, J. P., Zahniser, M. S., Worsnop, D. R., Knighton, W. B., Aiken, A.
618 C., Gorkowski, K. J., Dubey, M. K., Allan, J. D., and Thornton, J. A.: Contribution of
619 Nitrated Phenols to Wood Burning Brown Carbon Light Absorption in Detling, United
620 Kingdom during Winter Time, *Environ. Sci. Technol.*, 47, 6316-6324,

621 <https://doi.org/10.1021/es400683v>, 2013.

622 Ren, Y., Wei, J., Wang, G., Wu, Z., Ji, Y., and Li, H.: Evolution of aerosol chemistry in Beijing
623 under strong influence of anthropogenic pollutants: Composition, sources, and secondary
624 formation of fine particulate nitrated aromatic compounds, *Environ. Res.*, 204, 111982,
625 <https://doi.org/10.1016/j.envres.2021.111982>, 2022.

626 Ren, Y., Wang, G., Tao, J., Zhang, Z., Wu, C., Wang, J., Li, J., Wei, J., Li, H., and Meng, F.:
627 Seasonal characteristics of biogenic secondary organic aerosols at Mt. Wuyi in Southeastern
628 China: Influence of anthropogenic pollutants, *Environ. Pollut.*, 252, 493-500,
629 <https://doi.org/10.1016/j.envpol.2019.05.077>, 2019.

630 Salvador, C. M. G., Tang, R., Priestley, M., and Hallquist, M.: Ambient nitro-aromatic
631 compounds -biomass burning versus secondary formation in rural China, *Atmos. Chem.*
632 *Phys.*, 21, 1389-1406, doi.org/10.5194/acp-21-1389-2021, 2021.

633 Teich, M., Van Pinxteren, D., Wang, M., Kecorius, S., Wang, Z., Müller, T., Mocnik, G., and
634 Herrmann, H.: Contributions of nitrated aromatic compounds to the light absorption of
635 water-soluble and particulate brown carbon in different atmospheric environments in
636 Germany and China, *Atmos. Chem. Phys.*, 17, 1653-1672, [https://doi.org/10.5194/acp-17-](https://doi.org/10.5194/acp-17-1653-2017)
637 [1653-2017](https://doi.org/10.5194/acp-17-1653-2017), 2017.

638 Wang, G., Zhou, B., Cheng, C., Cao, J., Li, J., Meng, J., Tao, J., Zhang, R., and Fu, P.: Impact
639 of Gobi desert dust on aerosol chemistry of Xi'an, inland China during spring 2009:
640 differences in composition and size distribution between the urban ground surface and the
641 mountain atmosphere, *Atmos. Chem. Phys.*, 13, 819-835, [https://doi.org/10.5194/acp-13-](https://doi.org/10.5194/acp-13-819-2013)
642 [819-2013](https://doi.org/10.5194/acp-13-819-2013), 2013.

643 Wang, G., Zhang, R., Gomez, M. E., Yang, L., Levy, Z. M., Hu, M., Lin, Y., Peng, J., Guo, S.,
644 and Meng, J.: Persistent sulfate formation from London Fog to Chinese haze, *Proc Natl Acad*
645 *Sci U S A*, 113, 13630-13635, <https://doi.org/10.1073/pnas.1616540113/-/DCSupplemental>
646 2016.

647 Wang, G., Cheng, C., Huang, Y., Tao, J., Ren, Y., Wu, F., Meng, J., Li, J., Cheng, Y., Cao, J.,
648 Liu, S., Zhang, T., Zhang, R., and Chen, Y.: Evolution of aerosol chemistry in Xi'an, inland
649 China, during the dust storm period of 2013 – Part 1: Sources, chemical forms and formation
650 mechanisms of nitrate and sulfate, *Atmos. Chem. Phys.*, 14, 11571-11585,
651 <https://doi.org/10.5194/acp-14-11571-2014>, 2014.

652 Wang, H., Lu, K., Tan, Z., Chen, X., Liu, Y., and Zhang, Y.: Formation mechanism and control
653 strategy for particulate nitrate in China, *Journal of Environmental Sciences-China*, 123, 476-
654 486, 2023.

655 Wang, L., Wang, X., Gu, R., Wang, H., Yao, L., Wen, L., Zhu, F., Wang, W., Xue, L., Yang, L.,
656 Lu, K., Chen, J., Wang, T., Zhang, Y., and Wang, W.: Observations of fine particulate nitrated
657 phenols in four sites in northern China: concentrations, source apportionment, and
658 secondary formation, *Atmos. Chem. Phys.*, 18, 4349-4359, [https://doi.org/10.5194/acp-18-](https://doi.org/10.5194/acp-18-4349-2018)
659 [4349-2018](https://doi.org/10.5194/acp-18-4349-2018), 2018.

660 Wang, X., Gu, R., Wang, L., Xu, W., Zhang, Y., Chen, B., Li, W., Xue, L., Chen, J., and Wang,
661 W.: Emissions of fine particulate nitrated phenols from the burning of five common types
662 of biomass, *Environ. Pollut.*, 230, 405-412, <http://dx.doi.org/10.1016/j.envpol.2017.06.072>,
663 2017.

664 Wang, Y., Hu, M., Wang, Y., Zheng, J., and Yu, J. Z.: The formation of nitro-aromatic

665 compounds under high NO_x and anthropogenic VOC conditions in urban Beijing, China,
666 *Atmos. Chem. Phys.*, 19, 7649-7665, <https://doi.org/10.5194/acp-19-7649-2019>, 2019.

667 Wu, C., Wang, G., Li, J., Li, J., Cao, C., Ge, S., Xie, Y., Chen, J., Li, X., Xue, G., Wang, X.,
668 Zhao, Z., and Cao, F.: The characteristics of atmospheric brown carbon in Xi'an, inland
669 China: sources, size distributions and optical properties, *Atmos. Chem. Phys.*, 20, 2017-
670 2030, <https://doi.org/10.5194/acp-20-2017-2020>, 2020.

671 Xie, M., Chen, X., Hays, M. D., Lewandowski, M., Offenberg, J. H., Kleindienst, T. E., and
672 Holder, A. L.: Light Absorption of Secondary Organic Aerosol: Composition and
673 Contribution of Nitroaromatic Compounds, *Environ. Sci. Technol.*, 51, 11607-11616,
674 <https://doi.org/10.1021/acs.est.7b03263>, 2017.

675 Yi Chen, Penggang Zheng, Zhe Wang, Wei Pu, Yan Tan, Chuan Yu, Men Xia, Weihao Wang,
676 Jia Guo, Dandan Huang, Chao Yan, Wei Nie, Zhenhao Ling, Qi Chen, Shuncheng Lee, and
677 Wang, T.: Secondary Formation and Impacts of Gaseous Nitro-Phenolic Compounds in the
678 Continental Outflow Observed at a Background Site in South China, *Environ. Sci. Technol.*,
679 56, 6933-6943, <https://doi.org/10.1021/acs.est.1c04596>, 2022.

680 Yuan, B., Liggio, J., Wentzell, J., Li, S. M., and Stark, H.: Secondary formation of nitrated
681 phenols: insights from observations during the Uintah Basin Winter Ozone Study (UBWOS)
682 2014, *Atmos. Chem. Phys.*, <https://doi.org/10.5194/acp-16-2139-2016>, 2016.

683 Zhang, X., Lin, Y. H., Surratt, J. D., and Weber, R. J.: Sources, Composition and Absorption
684 ngstrm Exponent of Light-absorbing Organic Components in Aerosol Extracts from the Los
685 Angeles Basin, *Environ. Sci. Technol.*, 47, 3685-3693, <https://doi.org/10.1021/es305047b>,
686 2013.

687 Zhang, Y. Y., Müller, L., Winterhalter, R., Moortgat, G. K., Hoffmann, T., and Poschl, U.:
688 Seasonal cycle and temperature dependence of pinene oxidation products, dicarboxylic
689 acids and nitrophenols in fine and coarse air particulate matter, *Atmos. Chem. Phys.*, 10,
690 7859-7873, <https://doi.org/10.5194/acp-10-7859-2010>, 2010.

691